ADVANCED THEORY AND SIMULATIONS
www.advtheorysimul.com

Role of the Setae in an Ectoparasitic Seal Louse in Reducing Surface Drag: Numerical Modeling Approach

Anika Preuss, Stanislav N. Gorb, Alexander Kovalev, and Alexander E. Filippov*

***Echinophthirius horridus*, an ectoparasitic seal louse adapted for living on diving wildlife in the marine environment, exhibits unique cuticular morphology with dense body coverage of characteristically-shaped setae. This study investigates their potential role in reducing drag during the host's diving activities. Scanning electron microscopy (SEM) and confocal laser scanning microscopy (CLSM) examines *E. horridus* setae morphology, revealing stair-like elevations and gradual sclerotization increase from base to tip. Numerical simulations using movable cellular automata (MCA) demonstrate that optimal inclination of surface protrusions leads to vortex formation, potentially reducing friction and energy losses. Vertical protrusions cause stronger flow perturbations and higher energy dissipation compared to natural inclination. Over time, as flow self-organizes, total power losses decrease, suggesting natural selection optimized surface structure inclination and spacing to minimize friction and energy losses. Comparisons with shark scales reveal morphological similarities but different drag reduction mechanisms, with seal louse setae utilizing a "ball-bearing" effect and shark scales relying on a "riblet effect." This study provides insights into surface topography's influence on fluid dynamics at small scales, with potential applications in understanding biological surfaces and designing reduced surface drag artificial surfaces.**

1. Introduction

Insects have colonized almost every available habitat – whether air, water or land. With their incredible diversity and numbers, they are therefore the most successful animal group in terms of habitat diversity and number of species.[1] Their ability to thrive in different environments is largely due to specialized surface morphology, which has been shown to play an essential role in attachment, locomotion, and respiration.[2] Similar adaptations can also be found in other animal groups, such as fish, particularly sharks.[3–5] These surface structures have evolved to fulfill various biological functions, enhancing survival in specific ecological niches.

In sharks, scales are known as dermal denticles or placoid scales, which possess a tooth-like structure with a hard enamel-like outer layer and an inner core of pulp.[6,7] These scales provide several advantages, including protection by forming a tough, armored exterior that shields sharks from predators and physical damage,[4,8] defense against parasites and bacteria by making it difficult for them to attach to the shark's skin,[9,10] and improved hydrodynamic efficiency by reducing drag and turbulence, allowing sharks to swim more efficiently.[4] Insects, on the other hand, exhibit an even greater variety of surface structures, each adapted to fulfill specific functional roles. These structures contribute to coloration and patterning, as seen in the vibrant colors and intricate wing patterns of butterflies and moths, which aid in camouflage or mate attraction.[11,12] The microscopic architecture of the insect cuticle can create superhydrophobic surfaces, preventing water accumulation and ensuring dry respiratory openings.[13,14] Many insect surface structures also serve protective functions, forming physical barriers against environmental factors and potential predators.[15–18] Additionally, specialized setae act as mechanoreceptors, detecting air currents, vibrations, and physical contact, which are essential for navigation, predator avoidance, and food detection.[19,20] In some species, hair-like structures help regulate body temperature by trapping air close to the body,[21] while in pollinators like bees, specialized hairs aid in pollen collection and transport.[22,23] Furthermore, insects utilize hair-like structures on their feet for adhesion to smooth surfaces, improving locomotion,[24,25] and surface microstructures on wings influence aerodynamics, potentially enhancing flight efficiency.[26–28]

A rarer function of surface outgrowths in insects is the supply of air under water. While many insects rely on gills,[29–32] skin respiration,[33,34] siphons[35] or compressible gas gills,[29,36] a few insect species breathe under water via a so-called plastron. A plastron is a structure with a constant volume formed by a dense layer of superhydrophobic microstructures in various

A. Preuss, S. N. Gorb, A. Kovalev, A. E. Filippov
Department of the Functional Morphology and Biomechanics
University of Kiel
Am Botanischen Garten 1-9, 24118 Kiel, Germany
E-mail: apreuss@zoologie.uni-kiel.de

The ORCID identification number(s) for the author(s) of this article can be found under https://doi.org/10.1002/adts.202500429

DOI: 10.1002/adts.202500429

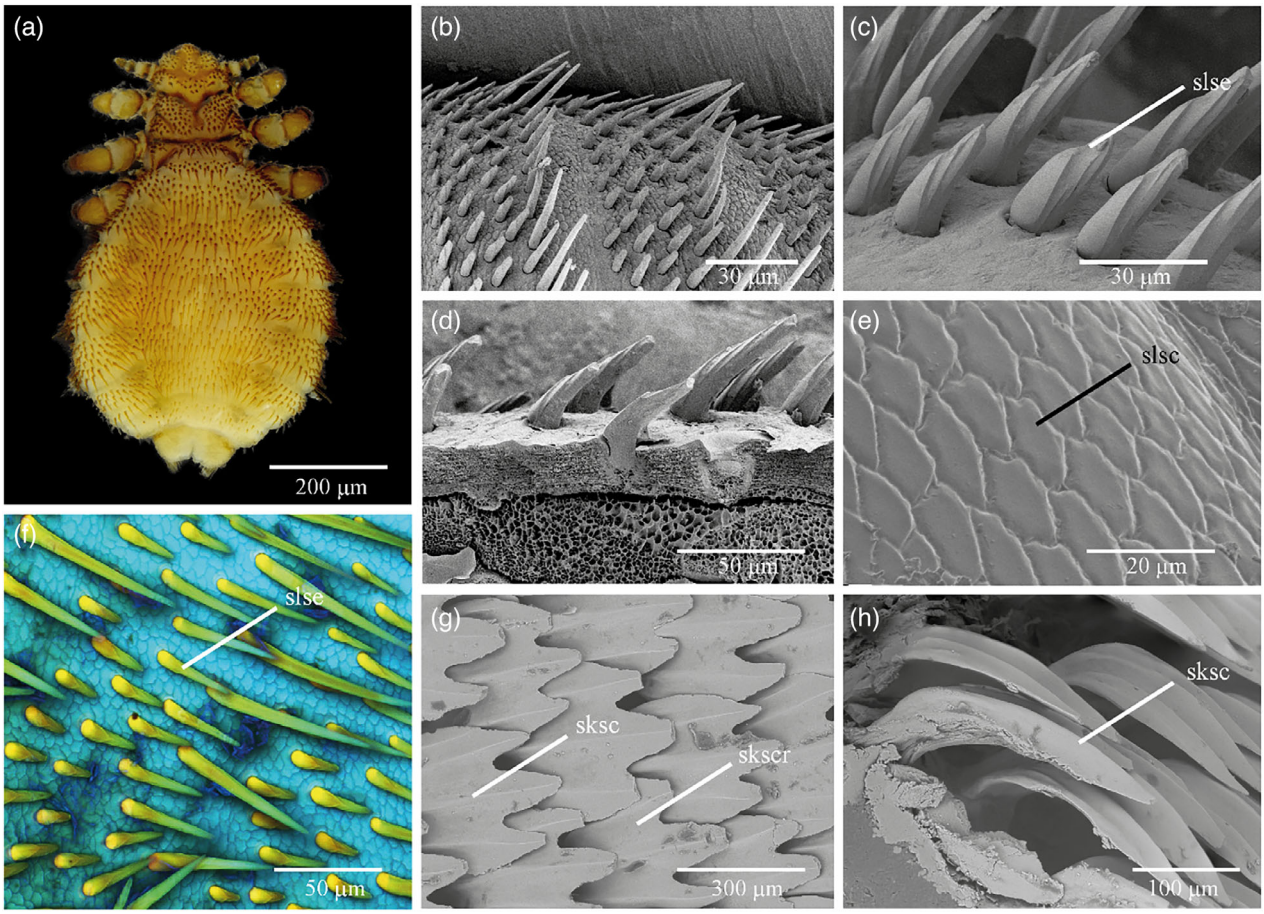

Figure 1. Outer morphology of seal louse setae and scales in comparison to porbeagle shark scales. A) Light photography of *E. horridus*. B–E) Scanning Electron Microscopy images of different surface structures of *E. horridus*: B) Different setae lengths on the dorsal side of the abdomen of *E. horridus*; C) Close-up of setae with stair-like elevations on their dorsal side; D) Cross-section through the cuticle and setae of *E. horridus* from lateral view; E) Top view on the dorsal abdominal scales of *E. horridus*. F) Confocal Laser Scanning Microscopy images of the setae and the cuticle of *E. horridus*. G,H) Scanning Electron Microscopy images of scales of *L. nasus*. G) Topview on scales from the lateral side of the shark; H) Lateral view on scales from the lateral side of the shark. Abbreviations: sksc (shark scale); slse (seal louse setae); slsc (seal louse scale).

forms, including small cuticle protrusions (microtrichia).[36–39] These structures typically possess bent tips and occur at densities sometimes exceeding 6 million cuticular protuberances per mm^2.[35] The superhydrophobic nature of these structures minimizes surface wettability, ensuring that the setal base and insect cuticle remain dry. This arrangement allows the insect's spiracles to maintain direct contact with the air film, facilitating continuous oxygen extraction from the water. Consequently, insects can remain submerged for extended periods.[38,40]

In the case of the seal louse, *Echinophthirius horridus* (Anoplura: Insecta), which parasites true seals (Phocidae), such as harbor seals (*Phoca vitulina*) and grey seals (*Halichoerus grypphus*), dense surface protuberances were also found on the cuticle.[41–44] It was assumed that these are either used for thermal insulation,[45] to hook into the fur of the seals[25,44] or could enable a plastron function.[36,46] It is therefore questionable what function dominates in surface microstructures of the seal louse.

To address this question, this study aims to (i) describe the general morphology of the setae and scales of *E. horridus* using imaging methods, such as SEM and CLSM, (ii) compare these with shark scales and (iii) analyze the turbulences at the cuticle surface covered by setae as a function of the inclination of the surface structure protrusions, when exposed to a constant flow using numerical modeling based on movable cellular automata (MCA).

This study provides insights into how surface topography influences fluid dynamics at small scales, with potential implications in understanding functional mechanisms of biological surfaces and designing artificial surfaces with efficient drag reduction.

2. Results

2.1. Outer Morphology

The body of the seal louse is largely covered with setae and scales (**Figure 1**A–F). Following Preuss et al. 2025 (under review), these setae have different lengths distributed over the body of the louse: in the middle of the individual abdominal segments, the setae are about 25 µm long, while at the transition points between the segments, they are up to 120 µm long and thus protrude beyond the grooves between individual segments. They form an angle of

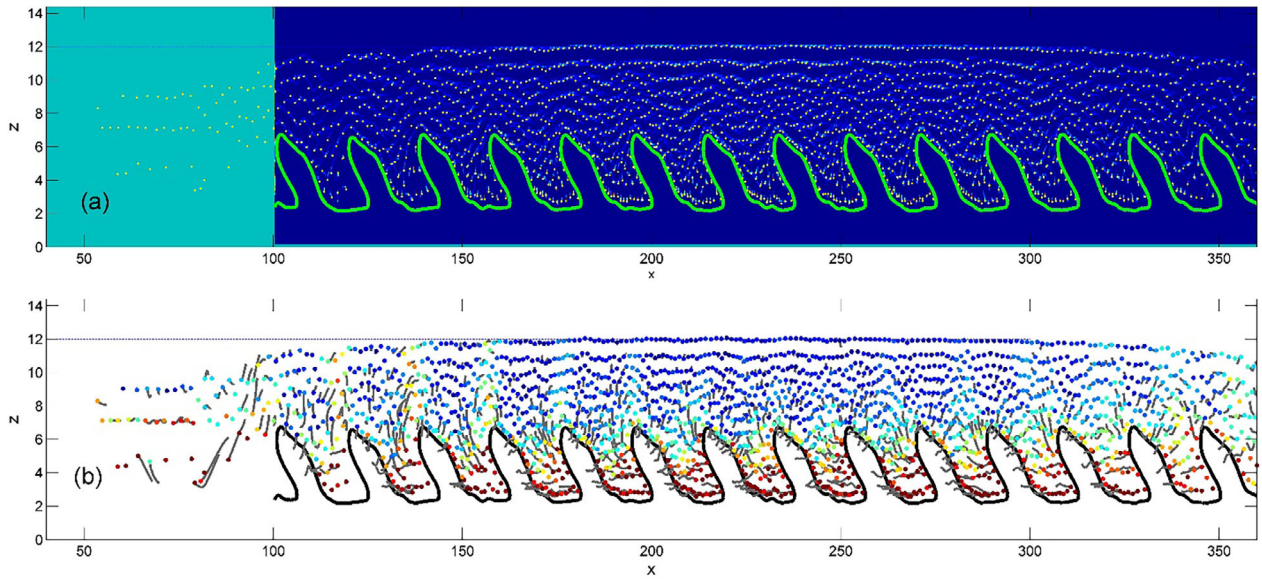

Figure 2. Typical instant configuration of the movable automata caused by motion of the rigid profile in horizontal direction. It is a snapshot of the self-organized stationary process, which appears after a transient process reproduced in the attached illustrative Movie S1, Supporting Information. Presence and absence of effective potential caused by the limited substrate is depicted by different background colors (deep and light blue) in the subplot (a). Green line shows current position of the surface. The same configuration in the subplot (b) shows scatter plot of automata colorized by absolute velocities of the particles. Standard MatLab "jet" colormap is used with deep red and blue colors for large and small values, respectively. Short parts of the automata trajectories are plotted by gray lines as "comet tails".

about 48° to the body surface of the lice and usually show three stair-like elevations on their dorsal side. The histological sections show that their anchoring extends far into the cuticle and also has a straight base. The setae exhibit a gradient of autofluorescence, transitioning from yellowish/orange at the base to greenish at the tip, indicating a gradual decrease in sclerotization. When examined in cross-section, the setae appear to be entirely composed of cuticle material, without internal spaces.

Echinophthirius horridus exhibits a distinctive scale-like pattern on its cuticle surface (Figure 1E), presenting the appearance of a body covered in plate-like protrusions resembling scales due to their orientation. Both cross-sectional and lateral views reveal that these "scales" do not actually overlap and the cuticle predominantly exhibits strong blue autofluorescence, suggesting them less sclerotized and relatively flexible.

In comparison, the placoid scales of the porbeagle shark, *L. nasus*, overlap considerably, so that almost half of each individual scale is covered by the previous one (Figure 1G,H). Each individual scale has the shape of a trident with groove-like substructures (ridges), each of which runs into a prong of this scale. Overall, however, the scales in lateral view with their straight base and their 30–35° angle to the body surface are strongly reminiscent of the shape of the setae in seal lice.

2.2. Numerical Simulation

With account of the dissipative term, the equations of motion assume the following form:

$$m\frac{\partial \mathbf{v}_i}{\partial t} = \mathbf{f}_i^{\mathrm{r}} - \eta \mathbf{f}_i^{\mathrm{v}} - \gamma \mathbf{v}_i + \xi(t, \mathbf{r}_i) \tag{1}$$

These equations were integrated using velocity Verlet's method, which conserves the energy of the system at each time step, provided no energy is supplied externally through the mechanical work or temperature variation. All the results obtained from the model are accumulated in Figures 2–8 and attached to the manuscript Movies S1–S7, Supporting Information. They are in details described below and briefly repeated in the captions to these figures, as well as in the descriptions to the movies.

Typical realization of an initial (transient) run and instant moment of system motion in the frames of discrete model is shown in **Figure 2**. Upper subplot (a) in this figure reproduces current positions of movable automata (yellow points) plotted together with boundary surface (shortly "substrate") depicted by bold green line. To make it possible, to simulate motion of the automata interacting with the substrate represented by multivalued function and having in some places negative inclination instead of the formal analytical funtion $Z_{down} = z_{down}(x)$, we used an effective boundary condition generated by a potential relief which exponentially grows inside the substrate.

It imposes some limitation on a size of the system used for the simulations. In Figure 2, this limitation is reporduced by different color of the background (deep and light blue). It means that particles outside of the deep blue region move without interaction with the substrate. It causes some boundary effects which, however, should exist for real system as well. To elucidate motion of the liquid particles in static picture, we use also short parts of their trajectories reproduced by means of so-called "comet tails". These tails are clearly seen in the subplot (b), as well as in the illustrative Movie S1, Supporting Information.

Let us mention also rather general tool, which was applied here, to visualize dynamics in the static pictures. The automata

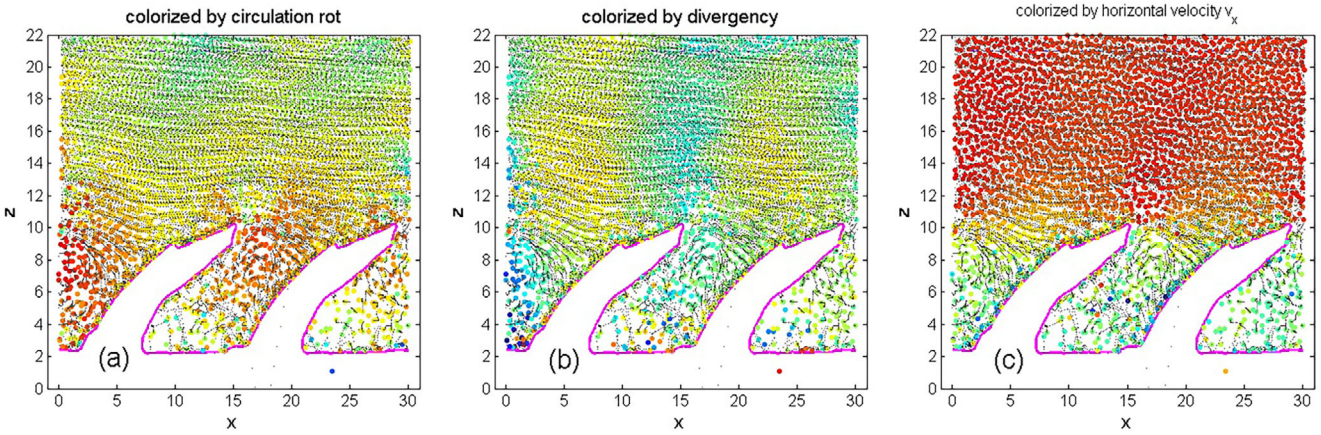

Figure 3. Two neighboring setae simulated with application of the "cylinder boundary conditions". The colorization in the subplots (a)–(c) corresponds to the values of local circulation, local divergence and horizontal velocity, respectively. Inclination angle: 48°.

moving in the model can be associated with their different physical properties simultaneously. Namely the same particle can be described by its vertical, horizontal and absolute velocity, can interact with the substrate and all other particles at once, as well as participate in the dissipation processes due to mutual exchange by their velocities and exchange by the energy with the thermostat.

All of these parameters are instantly visualized using standard MatLab "jet" colormap, colorized respectively to a particular value used for the colorization. In particular, such a colorization by absolute velocity of the particles is used in the conceptual plot shown in Figure 2. From this plot, one can directly see that particles moving with the velocities close to the velocity of transporting them substrate have higher absolute velocities (shown by deep red color) than the same particles, which practically do not move due to their location rather far from the substrate (deep blue ones).

One can note that sufficiently far from both (left and right) ends of the system, particles demonstrate more or less periodic behavior and their trajectories practically repeat the same patterns in different parts of the sufficiently long system. It allows us to cut out a short (repeated) internal part of the system and extend it periodically with a help of so-called "cylinder boundary conditions" and to simulate its behavior independently. This mathematical approach is well accepted in many theoretical and numerical investigations of friction considering particles placed on sufficiently long substrates (see for example Denisov et al., 2004, Filippov et al., 2023, 2024, Filippov and Gorb, 2020, Filippov and Estrin, 2023 and literature cited in them) and was applied in the present paper. It allowed us, to strongly reduce time consumption for the simulations and separate general results from the boundary effects, which are sometimes important but will be omitted here.

One has to note that such different motion velocities of different layers in the system under shear being accompanied by the viscosity (mutual friction between the particles of different velocity) is normally responsible for a generation of the vortices in the system.[62–68] In its turn, such vortices can lower integral friction and energy loses in the system, causing a kind of "ball-bearing" in it. One can expect that due to biological adaptation a substrate inclination and distance between the asperities can be properly adjusted to the typical velocities appearing in the system under consideration to lead to a minimization of the energy loses and drag.

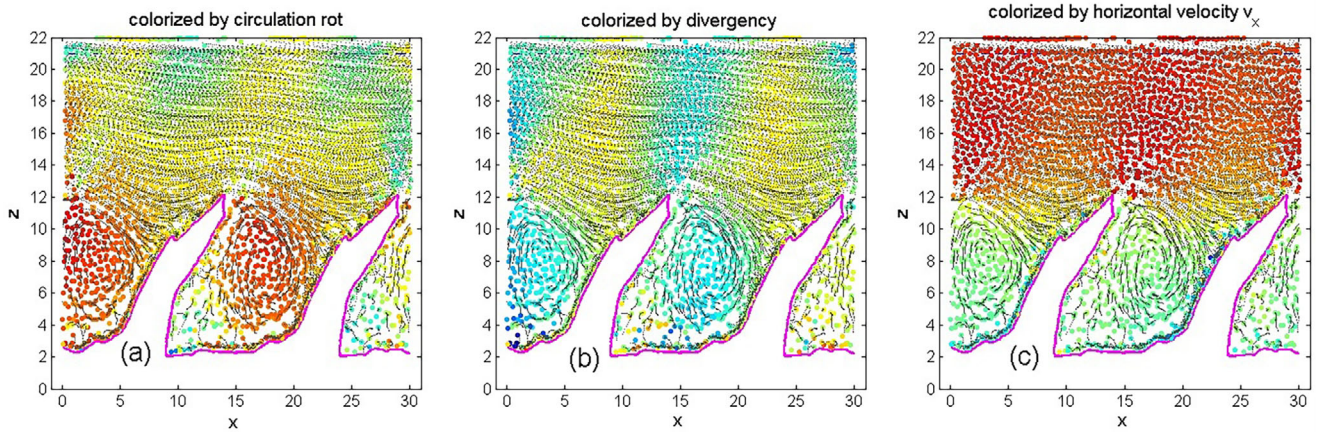

Figure 4. The same system as in Figure 3 with optimal inclination of the boundary structures. Inclination angle: 65°.

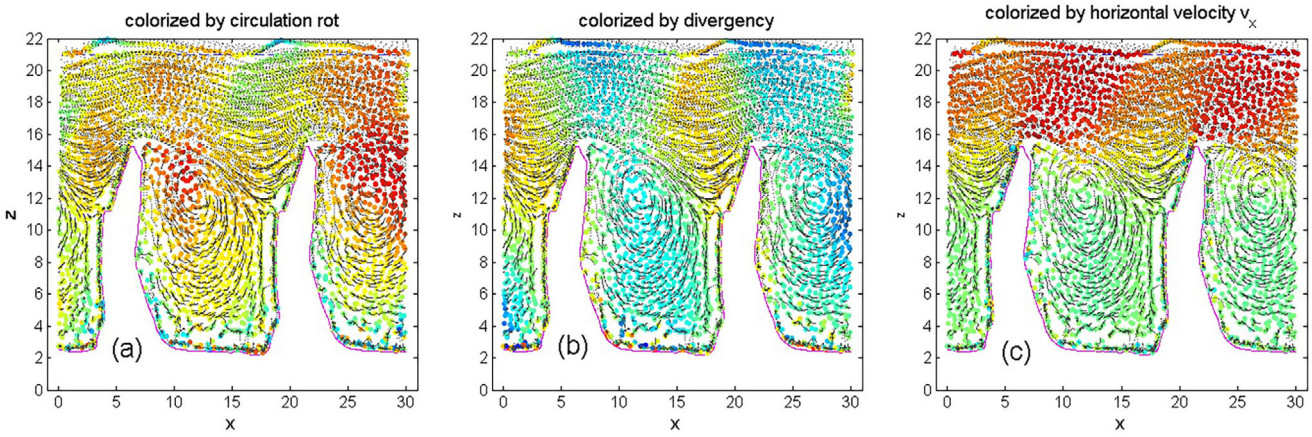

Figure 5. The same system as in Figure 3 with the vertically placed protrusions. Inclination angle: 90°.

Two spatial periods of qualitatively the same system simulated with application of the cylinder boundary conditions as the periodic (quasi-infinite) are shown in **Figure 3**. This simulation is done at small inclination of the setae relative to the substrate, which is smaller than actually observed in real (supposed to be optimal) system. The results are reproduced in convenient for the numerical simulation, so-called "following" system of the coordinates. It is associated with rigid substrate which remains immobile in these coordinates. The colorization in the subplots (a)-(c) corresponds to the values of local circulation (rotation in clockwise or opposite direction), local divergence (expansion or convergence of the flow lines) and horizontal velocity, respectively. In particular, it is seen that liquid quickly flows far from the substrate and almost stops near to the surface boundary.

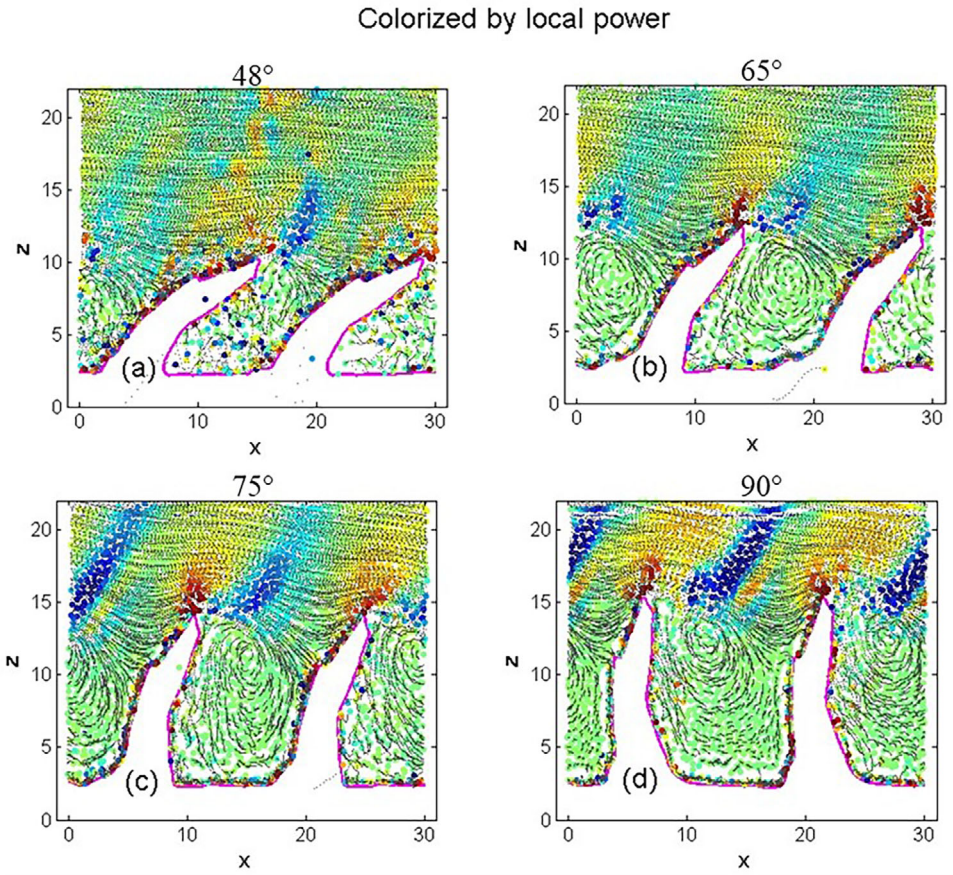

Figure 6. Local density of the power produced and consumed in the systems with different inclinations of setae. Inclination angles are shown above the graphs.

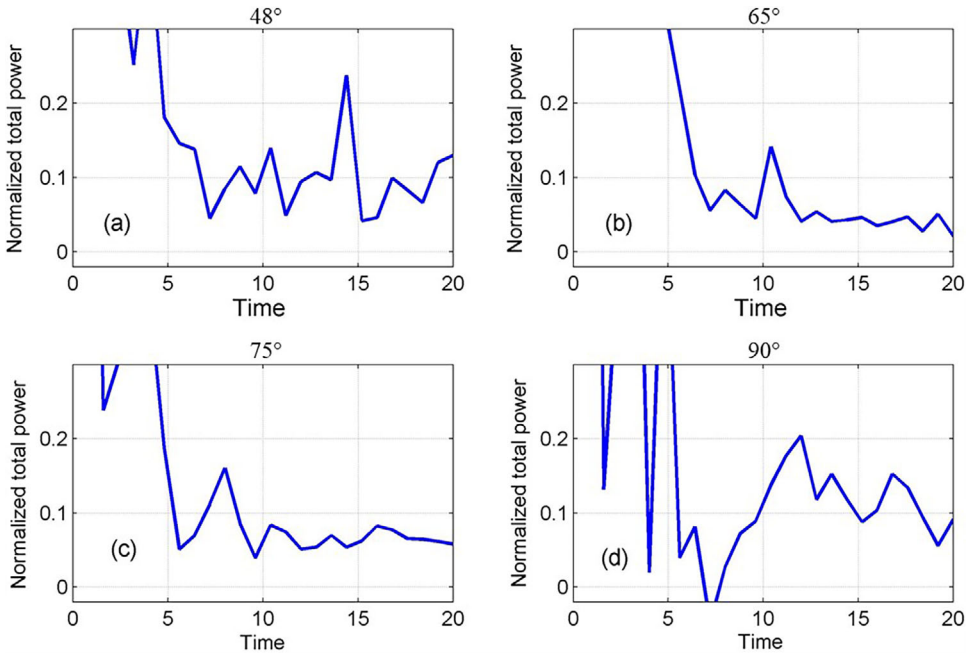

Figure 7. Time depending normalized total power in the four systems shown in Figure 6. Inclination angles are shown above the graphs.

Two setae with optimal inclination are shown in **Figure 4**. One can notice obvious difference with the previous figure. Clearly seen vortices are formed here between the protrusions of the surface. They are associated with the circular red spots in the rotor scatter plot depicted in the subplot (a). Corresponding rotation is also confirmed by the particle trajectories shown by gray lines. One can also see a correlation between the regions of rotation and density waves colorized by the divergence in the subplot (b). It is important to note that practically laminar flow conserves in the liquid moving above these structures, which separated by smooth boundary between them and outer region of the system in the subplot (c).

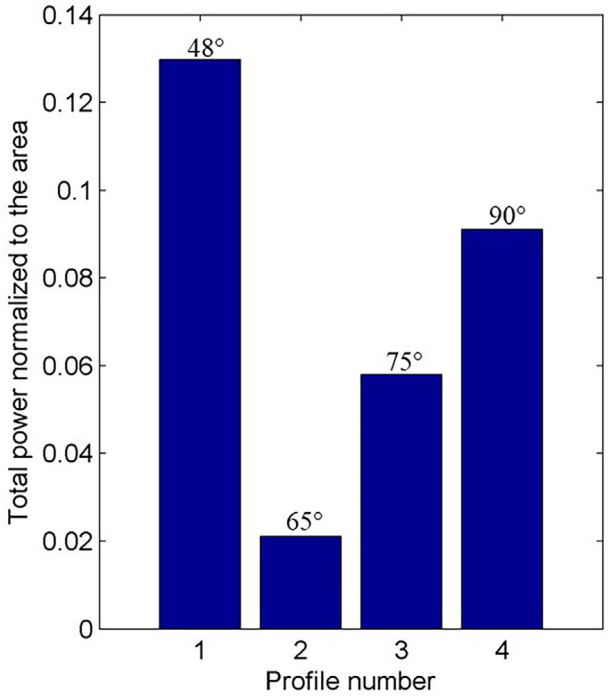

Figure 8. Averaged total power values for the systems with different inclinations shown in Figures 6 and 7 averaged over the intervals $10 < t < 20$ (after transient period has been passed). Inclination angles are shown above the graphs.

A simulation for the two setae artificially placed vertically in periodic boundary conditions are reproduced in **Figure 5**. The regions of the rotation are shifted here closer to the tops of the structure asperities. They cause stronger perturbations above them and, as expected, lead to the higher relative dissipation of dynamic energy in the system (**Figure 6**).

The results obtained for local density of the power produced and consumed in the systems with different inclinations of the substrate structure are summarized in Figure 6. These patterns of dissipation densities appear as self-organized ones at stationary stage of system evolution. They fluctuate with time and more or less regularly reproduced in dynamics of this turbulent system. Watching corresponding dynamics, one can visually observe that turbulent tails of the fluctuations are relatively smaller for the optimal inclination (b) than for the other ones (Supplementary Movie S7).

To support this quantitatively, we calculated normalized balance of total power in the system (**Figure 7**). Time depending normalized total power in all the four systems shown in Figure 6 is reproduced in corresponding subplots of Figure 7. It is clearly seen that in all the cases total energy loses in the system decrease in average with the time during transient self-organization process, but still continue to fluctuate. To compare the difference between total power in the above cases, we calculated averaged total power values for the systems with different setae inclinations averaged over sufficiently long-time intervals (after transient period

has been passed). The resulting bar plot shows typical values of total power calculated for sufficiently long run and averaged over mentioned fluctuations along time intervals $10 < t < 20$ in the subplots, where the process can be treated as almost stationary one (**Figure 8**). These results are shown below in the corresponding subplots of Figures 7 and 8.

3. Discussion

Seal lice have setae showing a very special shape and it has long been assumed that they either serve for thermal insulation,[45] for stronger adhesion to the seal's fur[25,44] and for facilitation of plastron breathing under water.[36,46] However, another function is also conceivable: the hairs could reduce drag, to which the lice are exposed during their hosts' dives.[70] Through our numerical simulations performed using digital automata model, we were able to demonstrate that the fluid flow over the setae creates vortices on the surface of the lice cuticle that promote a so-called "ball-bearing" effect, thereby lowering integral friction (drag) and energy loses in the system (Figure 2). As part of our morphological investigations, we recognized tear-like substructures that apparently "trap" these vortices and prevent them from dissolving prematurely (Figure 1C). The effect depends on the angle of the seta, with the optimal angle corresponding to the natural inclination of lice setae. This inclination is likely influenced by the resilin-containing socket at the base of each seta, which allows the setae to automatically adjust the angle, when exposed to the fluid drag (Figure 6). The experimentally observed spacing between the protrusions, as well as their inclination, both appear to be fine-tuned by natural selection to minimize surface drag, turbulence, and energy loss in the system.

At first glance, the shape of the setae resembles the scales of a shark, so that one might initially assume that it is a convergent development of similar mechanism of drag reduction (Figure 1G,H). However, a closer look at the shark scales reveals that they overlap considerably and that the physical effect in reducing the flow resistance is different and the "ball-bearing" effect observed in lice cannot take place in sharks. In sharks, the reduction in flow resistance is rather based on a collective riblet effect: the tiny longitudinal ridges on the scales of sharks that swim at high speeds function by hindering the lateral movement of longitudinal vortices within the viscous sublayer,[71] thereby resulting in a drag reduction of about 10% compared to smooth surfaces[71–76] and enhanced hydrodynamic performance in separating flows.[77,78] Therefore, in sharks, drag reduction primarily relies on the overlapping ridged scales, which generate laminar flow in the direction of swimming[79] (Figure 1G,H). Conversely, sea lice exhibit a "ball-bearing" effect observable at the gaps between individual seta, as these structures do not overlap (Figure 2).

If one compares the aquatic seal lice with terrestrial lice from the same order Anoplura, such as the human head louse *Pediculus humanus capitis*, the body louse *Pediculus humanus humanus*, the pubic louse *Pthirus pubis* or the cattle louse *Solenoptes capillatus*, a strong difference in the setal coverage of the bodies becomes visible: while the seal lice have an extremely dense coverage of 400 setae per square millimeter with different setal lengths depending on the body region,[80] only a few setae can be found on terrestrial louse species.[81–84] These are also primarily found in the antennal regions and the legs, so that it can be assumed that these setae have mainly a sensory function.[85,86] In addition, it can be deduced that the high density of setal distribution of seal lice could be an adaptation to their aquatic lifestyle and thus their habitat, as these are present in similar densities in all echinopthiriid taxa.[84,87] This supports our hypothesis that it is possibly an adaptation to the increased flow resistance under water.

In our calculations, we assumed that seal lice are fully exposed to the ambient flow. However, in reality, they are embedded within the seal's fur,[70] which offers some protection from the current and would consequently reduce the effective flow forces compared to our unprotected model scenario. This simplification may result in an overestimation of the actual flow resistance. Nonetheless, seal lice typically inhabit particularly exposed regions of the seal's body, such as the flippers and the head,[88–90] where fur coverage is sparser and local flow velocities remain relatively high. In these areas, adaptations to minimize flow resistance are especially crucial. Therefore, while our model represents an idealized scenario, it effectively captures the functional implications of surface topography under conditions likely pertinent to the natural habitat of the lice.

As can be seen from our SEM images, the setae of the seal lice have a specific orientation, in that they always point in a posterior direction (Figure 1B). Accordingly, it would be extremely disadvantageous from a fluid dynamics point of view, if the lice were positioned with their heads against the direction of flow, as this would create a "braking effect" through the setae and the vortices could not be built up. In previous studies, however, we have already observed that the seal lice on the seals always orient themselves with their heads toward the root of the seal hair when clinging to it.[70] The fact that the seal hair is naturally pressed flat against the seal body during the swimming process and the louse thus points its head in the direction of swimming means that the vortices can be built up and the flow resistance acting on the louse can be reduced. Thus, the orientation on the seal hair also creates more favorable flow conditions to the lice.[70,80] Additionally, the louse remains closer to the host surface with its mouthparts and does not have to reorient itself on the seal hair for the sucking process.[91,92]

It is questionable what influence a plastron would have on the flow resistance, if it could be built on the louse body, thanks to the setae.[80] Previous studies on air layers, which are found on biological or artificial systems under water, have already clearly shown that air layers on these surfaces act as a slip agent under water: when we consider solid surfaces, the flow velocity of the water directly on the surface is zero based on the friction between the water molecules and the solid surface.[93] If there is a layer of air between the water and the solid surface, the water simply flows over this air film. The viscosity of air is 55 times lower than that of water, so the air film can act as a slip agent and reduce drag.[93,94] Flow experiments have shown that the dorsal swimmer bug, *Notonecta glauca*, for example, uses an air film for drag reduction, which is made possible by the double structure of specifically-shaped setae and microtrichia, and that this remains stable even at higher flow velocities of up to 4.5 m s^{-1}.[39,93,95–97]

The so-called "Salvinia Effect" of the superhydrophobic floating fern (*Salvinia natans*) has already found various technical applications in the coating of ship hulls. *Salvinia natans* has a

surface covered by trichomes and can therefore build up an air film that can reduce drag in contact with water.[93,98] Therefore, such a plastron-like system would indeed contribute to drag reduction in the seal lice. However, previous studies have already shown that such a plastron does not exist in the seal lice, as the setal density of the lice is not sufficient and the shape of the setae is unsuitable for holding a plastron,[80] the plastron would no longer be stable above a diving depth of 30 m[99–101] and the lice apparently consume oxygen under water.[80] Accordingly, we can assume that the drag reduction, as shown in our simulations and calculations, is primarily based on the formation of vortices between the individual setae of the lice (Figure 2).

In summary, the unique shape and arrangement of the setae in the seal lice suggests that they are an adaptation to their extreme living environment. Our simulations have shown that the optimal inclination of surface protrusions (setae) leads to formation of vortices that may reduce drag and energy losses in an aquatic environment. Furthermore, the vertical protrusions cause stronger flow perturbations and likely higher energy dissipation and the total power losses in the system decrease over time as the flow self-organizes. This suggests that natural selection may have optimized surface structure inclination and spacing, to minimize drag and energy losses in the seal lice. Finally, this study provides insights into surface topographies that influence fluid dynamics at small scales with potential implication to understanding biological surfaces on one side and to designing drag-reducing biomimetic surfaces.

4. Experimental Section

Samples: For morphological analysis, seal lice specimens were collected from harbor seals at the Seal Centre Friedrichskoog between June and September 2023. This facility is the sole authorized institution in Schleswig Holstein for the admission, rearing, and rehabilitation of abandoned and ill seals. The collection of seal lice at the center was conducted using non-invasive methods, specifically lice combs and forceps, during routine medical procedures. This methodology was selected to minimize stress and reduce unnecessary handling time for the seals. Subsequently, the collected seal lice specimens were preserved in 70% ethanol solution. Shark skin (*Lamna nasus*) was kept in a dried state in the specimen collection of Zoological Institute at the CAU Kiel.

Confocal Laser Scanning Microscopy: For CLSM analysis, seal lice were immersed in glycerine (≥99.5%) and covered with a precision cover slip (thickness = 0.170 ± 0.005 mm, refractive index = 1.52550 ± 0.00015, Carl Zeiss Microscopy GmbH, Jena, Germany) prior to scanning. Autofluorescence of the specimens was examined using a CLSM Zeiss LSM 700 coupled to an upright Zeiss Axio Imager microscope (Carl Zeiss Microscopy GmbH, Jena, Germany). The examination employed four solid-state lasers (wavelengths 405, 488, 555, and 639 nm) and their corresponding emission filters (BP420–480, LP490, LP560, LP640 nm). Following the methodology described by Michels & Gorb (2012), the 405 nm excitation and 420–480 nm emission filter highlighted less sclerotized cuticle, potentially rich in resilin. Regions of higher sclerotization were detected using 488 nm and 555 nm laser excitations with filters that permitted emission light above 490 and 560 nm, respectively. The 639 nm laser excitation with a 640 nm long-path emission filter captured extended autofluorescence. Images taken at different settings were superimposed using ZEN 2008 software (www.zeiss.de/mikroskopie) and Adobe Photoshop CS6 (Adobe Photoshop CS, San José, USA) for qualitative, but not quantitative, assessment of cuticle composition.[47–51] In the autofluorescence images, specific colors correspond to particular material properties:[49] Reddish autofluorescence indicates highly sclerotized cuticle, with more intense red hues denoting greater degrees of sclerotization. Greenish autofluorescence suggests relatively resilient cuticle with high chitin content, while bluish autofluorescence signifies softer, less-sclerotized cuticle regions, often containing rubber-like protein resilin.

Scanning Electron Microscopy: Mature seal lice (n = 4) underwent dehydration utilizing a series of increasing alcohol concentrations, followed by critical point drying in a Leica EM CPD300 (Leica, Wetzlar, Germany) automated system. The specimens and pieces of dried shark skin were subsequently sputter-coated with a 10 nm layer of gold-palladium using a Leica Bal-TEC SCD500. Samples were examined from different angles of view using a Hitachi TM3000 (Hitachi Ltd., Tokyo, Japan) with a rotatable sample holder at 15 kV acceleration voltage.[52] To investigate the surface morphology in detail in freshly-killed lice, cryo-scanning electron microscopy (SEM) was employed. Lice were frozen in a cryo stage preparation chamber at −140 °C (Gatan ALTO 2500 cryo preparation system, Gatan Inc., Abingdon, UK). The frozen specimens were then sputter-coated with a 6 nm layer of gold-palladium and observed using a SEM Hitachi S-4800 (Hitachi Ltd., Tokyo, Japan) at 3 kV accelerating voltage and −120 °C cryostage temperature. The resulting images were enhanced utilizing Adobe Photoshop CS6 (Adobe Photoshop CS, San José, USA) and Affinity Photo 1.10.6 (Serif Ltd, Nottingham, UK).

Numerical Model: Dynamic behavior of the fluids moving in contact with rigid surfaces having various spatial profiles can be simulated by the method of movable cellular automata (MCA). Depending on chemical composition and temperature this substance can be gaseous, liquid or even solid (particulate). MCA approach was well established to present time and was relatively simple. In majority of practically important cases, it was proven to be less time consuming than other calculation methods and rather universal. It was useable in different systems at changeable conditions which even pass from some initial physical states to new ones. The model structure in the present paper generally repeats analogous models already used in large number of previous works.[53–69] Thus, for details of the numerical approach this work can address the reader to the previous works, but will reproduce the model briefly, only for a convenience of the reading.

In movable automata approach, one deals with a system of N movable objects (effective "particles"). As usually in dynamics, they a represented by the vector radius r_i, the momentum p_i, and the interaction potential $U(|r_i - r_j|)$ corresponding to the following Hamiltonian (see for example Landau and Lifshitz, 1976):

$$H(r_i, p_i) = \sum_{i=1}^{N} p_i^2/2m + \sum_{i,j=1}^{N} U(|r_i - r_j|)/2 \tag{2}$$

The main idea is to simulate liquid (gas) using simple interaction potential defined by a pair of the Gauss potentials:

$$U(|r_i - r_j|) = C_{ij} \exp\{-[(r_i - r_j)/c_{ij}]^2\} - D_{ij} \exp\{-[(r_i - r_j)/d_{ij}]^2\} \tag{3}$$

where C_{ij} and D_{ij} define the magnitude, while c_{ij} and d_{ij} the radii of attraction and repulsion, and relation between the parameters: $C_{ij} >> D_{ij}$, $c_{ij} < d_{ij}$. The equations of motion have the following form:

$$m\partial v_i/\partial t = -\partial H(r_i, p_i)/\partial r_i + f_i \tag{4}$$

v_i is the velocity of the i-th particle, are the forces f_i will be explained further.

All the unknown or stochastic influences inherent in any biological system should be incorporated according to fluctuation-dissipation theorem with effective temperature T_{eff}. As usually, it was simulated by random δ-correlated Langevin forces, having the correlators:

$$\left\langle \xi(t, r_i)\xi(t', r_j) \right\rangle = D\delta(t - t')\delta_{ij} \tag{5}$$

where $\langle \xi(t, r_i) \rangle = 0$ and diffusion coefficient is proportional to temperature $D \sim T$.

For the particular study, it was important to note that by varying intensity of noise at fixed interactions or vice versa, the system could represent different states: from gaseous to liquid and solid ones[1–7] Below, this work will always suppose that this relation is chosen to simulate *liquid*.

There were different options to simulate numerically the liquid motion near to solid interfaces. For example, in the simplest case, the liquid can be confined between two planar rigid repulsing planes: $z = z_{down}$ (lower plane) and $z = z_{up} \equiv L_z$ (upper plane). Numerically, it can be done by means of reflecting boundary conditions with sharp repulsing potentials exponensially growing inside the boundary walls:

$$U_{up} = C\exp[(z - L_z)/c] \text{ and } U_{down} = C\exp[(z_{down} - z)/c] \quad (6)$$

Here the constants C and c without indices denote repulsion from the boundaries, different from the repulsion between the particles described by the values C_{ij} and c_{ij}. To simulate rigid contact surfaces, one needs to apply strong inequalities $C >> C_{ij}$ and $c << c_{ij}$.

In more general case of the profiled substrates, the planes should be substituted by some functions $Z_{up} = f_{up}(z)$ and $Z_{down} = f_{down}(z)$. Let us consider the upper boundary here as a formal planar boundary with potential $U_{up} = C\exp[(z - L_z)/c]$. One can treat the automata at the upper bondary (that are rather far from the movable substrate) as practicaly immobile $v_x(y = L_z) \approx 0$. It was aplicable in the case, when the system was actually open (infinite) perpendicular to the fluid flow. It meant that this work ajusted a height of the liquid layer to keep mean density of the liquid $< \rho >$ inside the layer Ω (approximately) fixed $< \rho > \approx const$. The higher upper boundry was placed (formally $L_z \to \infty$), the better model reproduces reality (Figure 2).

The particular configuration, which this work will study below, involved lower boundary surface with different and even negative inclination (Figure 2). Since the lower boundary was a multivalued function of coordinate x, it was not possible to describe the boundary using an analytical funtion $Z_{down}(x) = z_{down}(x)$ and a special procedure described further was applied for the boundary condition. An effective boundary, determined by 2D potential relief $U = u_{down}(x, z)$, which exponentially tended to infinity inside the lower substrate $z = z_{down}(x)$ and fell down to zero outside the substrate, defines the boundary by itself by a contour $u_{down}(x, z) = +0$. Such a contour was always used in the figures below, to depict profiled rigid down surface $u_{down}(x, z) = +0$.

As a result, the movable automata ("particles") naturally repulse from such a "surface" in correct direction independently on the surface inclination. It happened due to the simultaneous action of both vector components of the gradient: $\partial U/\partial x$ and $\partial U/\partial z$. The only sufficiently sharp 2D potential (exponentially growing inside the lower substrate) was nesessary to reproduce rather relistic dynamics of the system.

This work used two types of bondary conditions in x-drection: 1) the liquid was either confined inside a box, sufficiently long to include complete system inside (with sufficiently large amount of liquid around, to reproduce the system realistically), or 2) the system was periodically extended along horizontal coordinate. Such an extension can simulate quasi-infinite space as well.

In a case of horizontally long system without periodic extension the above-mentioned boundary conditions should repulse the particles by left and right boundaries of an imaginary box $U_{left/right} = C\exp\{[x - (L_x/2 \pm l_x)]/c\}$, where characteristic width of the surface structures is much smaller than the system size $L_x >> l_x$ (Figure 2). In periodically continued system, the particles were forced to "return back" to other side of the box each time, when they leave it, and continue their motion in the same direction. Besides, the particles close to one side not only interact with surrounding particles, they also interact with the "images" of the particles on opposite side of the box. This was an implementation of so-called "cylinder boundary conditions" which normally used in literature to simulate an "infinte system". Below this work applied both variants to illustrate a role of the liquid boundaries in the first case, and in the second case to simulate an internal behaviour of the system in the regions situated distantly from the boundaries, where the system can be approxiately treated as practically "endless".

A dissipation channel of the interaction between particles was certainly important in any simulation of liquid as well. Normally it tended to equilibrate the relative velocities of the particles. This work introduced such dissipation into the model with some characteristic interaction distance c_v comparable with effective size of the particles (their repuslion cores, $c_v \simeq c_{ij}$. Technically, in the frames of the movable automata approach, it was done by including a velocity-dependent additional force:

$$f_i^v = \eta\sum_{j=1}^{N}\{(v_i - v_j)exp[-[((r_i - r_j))/c_v]^2] + v_i exp[-(z_i/c_v)^2] + (v_i - v_{up})exp[-[((z_i - z_{up}))/c_v]^2]\} \quad (7)$$

acting on the i-th particle, with yet another dissipation constant η.

When some automata appear close in phase space (coordinates and velocities), they can aggregate one with another for a while into effective drops. This aggregation was caused by a balance between repulsing and attracting forces, which tends to conserve mutual distance between the particles close to a minimum of total potential determined by combination of the attracting

$$U_{attract}(|r_i - r_j|) = -D_{ij}\exp\{-[(r_i - r_j)/d_{ij}]^2\} \quad (8)$$

and repulsing

$$U_{repulse}(|r_i - r_j|) = C_{ij}\exp\{-[(r_i - r_j)/c_{ij}]^2\} \quad (9)$$

components of the potential $U(|r_i - r_j|)$. It leads to a collective behaviour responsible for the formation of vortices, turbulence and total loses in the system, discussed in the next section of the paper.

Numerical simulations were performed in MatLab (MathWorks).

Supporting Information

Supporting Information is available from the Wiley Online Library or from the author.

Acknowledgements

The authors extend their gratitude to Dr. Thies Büscher, Helen Gorges, Fabian Bäumler, Julian Thomas, Simon Züger, and Benedikt Josten for their support throughout this research. Additionally, the authors appreciate Esther Appel's technical support with collecting morphology data. The authors also express their thanks to the personnel at the Seal Centre Friedrichskoog and Dr. David Ebmer from Vienna Zoo for their excellent cooperation in sampling and providing seal lice. The authors are deeply appreciative of the financial support provided to S.N.G. through the grant GO 995 46-1 from the German Science Foundation (DFG) within the Special Priority Program (SPP 2332) "Physics of Parasitism". It is important to note that the funding bodies had no involvement in the study's design, data collection and analysis, publication decisions, or manuscript preparation.

Conflict of Interest

The authors declare no conflict of interest.

Author Contributions

A.F. created the numerical model, which was validated by A.P., S.G. and A.K. A.F. and A.P. created illustrations. AP studied the model object, made observations, and measurements. A.F. and A.P. wrote the manuscript. All co-authors revised the manuscript.

Data Availability Statement

The data that support the findings of this study are available from the corresponding author upon reasonable request.

Keywords

biomechanics, fluid dynamics, marine mammals, movable automata, parasitism

Received: March 6, 2025
Revised: May 8, 2025
Published online: June 9, 2025

[1] D. Grimaldi, M. S. Engel, *Evolution of the Insects*, Cambridge University Press, Cambridge, England, **2005**.
[2] C. Wan, S. Gorb, *J. Comp. Physiol. A* **2023**, *209*, 215.
[3] O. Hertwig, *Jena. Z. Naturw.* **1874**, *8*, 331.
[4] W. Raschi, C. Tabit, *Mar. Freshwater Res.* **1992**, *43*, 123.
[5] H. Ghiradella, *Adv. Insect Physiol.* **2010**, *38*, 135.
[6] R. L. Cooper, E. F. Nicklin, L. J. Rasch, G. J. Fraser, *Evol. Dev.* **2023**, *25*, 54.
[7] E. F. Nicklin, K. E. Cohen, R. L. Cooper, G. Mitchell, G. J. Fraser, *Dev. Biol.* **2024**, *516*, 221.
[8] E. J. Southall, D. W. Sims, *Proc. R. Soc. B* **2003**, *270*, 47.
[9] M. Lee, *Remarkable Nature Material Surfaces and Their Engineering Potential*, Springer, Berlin, **2013**.
[10] Y. L. Peng, C. G. Lin, L. Wang, *Adv. Mater. Res.* **2009**, *79–82*, 977.
[11] M. Srinivasarao, *Chem. Rev.* **1999**, *99*, 1935.
[12] B. D. Wilts, A. Matsushita, K. Arikawa, D. G. Stavenga, *J. R. Soc. Interface* **2015**, *12*, 20150717.
[13] G. S. Watson, B. W. Cribb, J. A. Watson, *J. Struct. Biol.* **2010**, *171*, 44.
[14] J. A. Watson, H.-M. Hu, B. W. Cribb, G. S. Watson, *On Biomimetics*, IntechOpen, London, **2011**.
[15] T. Eisner, J. Shepherd, *Ann. Entomol. Soc. Am.* **1966**, *59*, 868.
[16] T. Eisner, R. Alsop, G. Ettershank, *Science (80-.)* **1964**, *146*, 1058.
[17] S. Sugiura, K. Yamazaki, *Behav. Ecol.* **2014**, *25*, 975.
[18] A. Kageyama, S. Sugiura, *Sci. Nat.* **2016**, *103*, 86.
[19] M. Gewecke, *Experimental Analysis Of Insect Behaviour*, Springer Nature, United States, **1974**, pp 100–113.
[20] S. B. McIver, *Annu. Rev. Entomol.* **1975**, *20*, 381.
[21] B. Heinrich, *Science (80-.)* **1974**, *185*, 747.
[22] Z. M. Portman, M. C. Orr, T. Griswold, *J. Hymen. Res.* **2019**, *71*, 171.
[23] R. W. Thorp, *Plant Syst. Evol.* **2000**, *222*, 211.
[24] Z. Liu, S. N. Gorb, H. Liang, M. Bai, Y. Lu, *Insects* **2024**, *15*, 650.
[25] S. N. Gorb, *Integr. Comp. Biol.* **2002**, *42*, 1127.
[26] T. Engels, D. Kolomenskiy, F. O. Lehmann, *J. R. Soc. Interface* **2021**, *18*, 20210518.
[27] W. Nachtigall, *Z. Vergl. Physiol.* **1967**, *54*, 210.
[28] N. Slegers, M. Heilman, J. Cranford, A. Lang, J. Yoder, M. L. Habegger, *Bioinspiration Biomimetics* **2017**, *12*, 016013.
[29] V. B. Wigglesworth, *The Principles of Insect Physiology*, Springer Nature, Methuen, **1953**, p. 827.
[30] C. H. Eriksen, *J. North Am. Benthol. Soc.* **1986**, *5*, 16.
[31] U. Norling, *Zool. Jahrb. Abt. Anat. Ontog. Tiere* **1982**, *7*, 343.
[32] K. Suzuki, Y. Watanabe, K. Tojo, *Entomol. Sci.* **2020**, *23*, 280.
[33] G. Fraenkel, G. V. B. Herford, *J. Exp. Biol.* **1938**, *15*, 266.
[34] K. K. Jones, S. J. B. Cooper, R. S. Seymour, *J. Exp. Biol.* **2019**, *222*, jeb196659.
[35] C. H. Eriksen, G. A. Lamberti, V. H. Resh, *Aquatic Insect Respiration. An Introduction to the Aquatic Insects of North America*, Vol. *3*, Kendall/Hunt Publishing Co, Dubuque, **1996**, pp. 29–40.
[36] H. E. Hinton, *Mar. Insects* **1976**, *43*, 79.
[37] E. A. Hebets, R. F. Chapman, *J. Insect Physiol.* **2000**, *46*, 13.
[38] W. H. Thorpe, *Biol. Rev.* **1950**, *25*, 344.
[39] A. Balmert, H. Florian Bohn, P. Ditsche-Kuru, W. Barthlott, *J. Morphol.* **2011**, *272*, 442.
[40] M. R. Flynn, J. W. M. Bush, *J. Fluid Mech.* **2008**, *608*, 275.
[41] L. A. Durden, G. G. Musser, *Bull. Am. Mus. Nat. Hist.* **1994**, 1.
[42] M. S. Leonardi, R. L. Palma, *Zootaxa* **2013**, *3630*, 445.
[43] B. Grzimek, *Grzimek's Encyclopedia of Mammals*, McGraw-Hill Publishing Company, New York, **1990**.
[44] T. White, I. Mikó, *bioRxiv* **2024**.
[45] B. Mehlhorn, H. Mehlhorn, J. Plötz, *Parasitol. Res.* **2002**, *88*, 651.
[46] G. Enderlein, *Zool. Anz.* **1906**, *29*, 659.
[47] S. O. Andersen, *Annu. Rev. Entomol.* **1979**, *24*, 29.
[48] J. F. V. Vincent, *Composites, Part A* **2002**, *33*, 1311.
[49] J. Michels, S. N. Gorb, *J. Microsc.* **2012**, *245*, 1.
[50] S. Büsse, S. N. Gorb, *R. Soc. Open Sci.* **2018**, *5*, 172117.
[51] B. Josten, S. N. Gorb, S. Büsse, *J. Morphol.* **2022**, *283*, 1163.
[52] H. Pohl, *Microsc. Res. Tech.* **2010**, *73*, 1073.
[53] J. R. Pasta, *Comput. Phys. Commun.* **1972**, *3*, 139.
[54] S. M. Ulam, in *Problems in Modern Mathematics*, Dover Publications, Mineola, New York, United States, **1960**, pp. 115–141.
[55] E. Fermi, J. R. Pasta, S. M. Ulam, *Collect. Work.* **1955**, *2*, 978.
[56] P. Langevin, *C.R. Acad. Sci. Paris* **1908**, *146*, 530.
[57] L. D. Landau, E. M. Lifshitz, *Mechanics*, Course of Theoretical Physics, Vol. 1, Pergamon Press, **1976**.
[58] S. Denisov, A. Filippov, J. Klafter, M. Urbakh, *Phys. Rev. E* **2004**, *69*, 42101.
[59] A. E. Filippov, K. Nadein, S. N. Gorb, A. Kovalev, *Tribol. Lett.* **2023**, *72*, 11.
[60] A. E. Filippov, K. Nadein, S. N. Gorb, A. Kovalev, *Adv. Theory Simulations* **2024**, *7*, 2400348.
[61] A. Filippov, S. Gorb, *Combined Discrete and Continual Approaches in Biological Modelling*, Springer Cham, Cham, Switzerland, **2020**, p. 137.
[62] A. Filippov, V. Popov, *Facta Univ., Ser. Mech. Eng.* **2023**, *21*, 553.
[63] Y. Beygelzimer, A. Filippov, Y. Estrin, *Philos. Mag.* **2023**, *103*, 1017.
[64] Y. Beygelzimer, Y. Estrin, A. Filippov, A. Mazilkin, M. Mail, B. Baretzky, R. Kulagin, *Mater. Lett.* **2022**, *324*, 132689.
[65] W. Österle, A. I. Dmitriev, H. Kloß, *Tribol. Int.* **2012**, *48*, 128.
[66] W. Österle, A. Dmitriev, H. Kloß, *Tribol. Lett.* **2014**, *54*, 257.
[67] R. E. D. Rudge, J. P. M. van de Sande, J. A. Dijksman, E. Scholten, *Soft Matter* **2020**, *16*, 3821.
[68] A. Alazemi, *Lubricants* **2021**, *9*, 81.
[69] W. B. Paul, *Adv. Mater.* **1993**, *5*, 223.
[70] A. Preuss, T. H. Büscher, I. Herzog, P. Wohlsein, K. Lehnert, S. N. Gorb, *Commun. Biol.* **2024**, *7*, 36.
[71] B. Dean, B. Bhushan, *Philos. Trans. R. Soc., London Ser. A* **2010**, *368*, 4775.
[72] J. Oeffner, G. V. Lauder, *J. Exp. Biol.* **2012**, *215*, 785.
[73] G. V. Lauder, D. K. Wainwright, A. G. Domel, J. C. Weaver, L. Wen, K. Bertoldi, *Phys. Rev. Fluids* **2016**, *1*, 060502.
[74] L. Wen, J. C. Weaver, G. V. Lauder, *J. Exp. Biol.* **2014**, *217*, 1656.
[75] D. W. Bechert, M. Bruse, W. Hage, *Exp. Fluids* **2000**, *28*, 403.
[76] C. J. Lloyd, K. Mittal, S. Dutta, R. M. Dorrell, J. Peakall, G. M. Keevil, A. D. Burns, *R. Soc. Open Sci.* **2023**, *10*, 220684.
[77] K. T. Du Clos, A. Lang, S. Devey, P. J. Motta, M. L. Habegger, B. J. Gemmell, *J. R. Soc. Interface* **2018**, *15*, 14.
[78] A. W. Lang, M. T. Bradshaw, J. A. Smith, J. N. Wheelus, P. J. Motta, M. L. Habegger, R. E. Hueter, *Bioinspiration Biomimetics* **2014**, *9*, 036017.
[79] A. G. Domel, M. Saadat, J. C. Weaver, H. Haj-Hariri, K. Bertoldi, G. V. Lauder, *J. R. Soc. Interface* **2018**, *15*, 20170828.

[80] A. Preuss, T. Schwaha, A. Kovalev, D. Ebmer, I. Herzog, K. Lehnert, C. Grass, F. Sandberg, E. Hamann, M. Zuber, T. van de Kamp, S. N. Gorb, *Commun. Biol.* accepted for publication (2025).
[81] B. E. Álvarez-Fernández, M. Morales-Suárez-Varela, B. Nogueda-Torres, M. A. Valero, *Parasites Vectors* **2021**, *14*, 577.
[82] E. Mey, *Rudolstädter naturhistorische Schriften* **2003**, *11*, 115.
[83] R. Wall, D. Shearer, *Veterinary Entomology*, Springer Dordrecht, Netherlands, **1997**, p. 456.
[84] K. C. Kim, H. W. Ludwig, *Syst. Entomol.* **1978**, *3*, 249.
[85] R. N. Singh, K. Singh, S. Prakash, M. J. Mendki, K. M. Rao, *Int. J. Insect Morphol. Embryol.* **1996**, *25*, 183.
[86] J. M. Schmidt, J. J. B. Smith, P. A. Lawrence, *Proc. R. Soc. London, Ser. B* **1997**, *232*, 323.
[87] F. J. Aznar, M. S. Leonardi, B. B. Vera, D. G. Vales, S. Ameghino, J. A. Raga, E. A. Crespo, *Parasitology* **2009**, *136*, 293.
[88] G. Aarts, S. Brasseur, J. J. Poos, J. Schop, R. Kirkwood, T. van Kooten, E. Mul, P. Reijnders, A. D. Rijnsdorp, I. Tulp, *Ecosphere* **2019**, *10*, 02538.
[89] I. Herzog, U. Siebert, K. Lehnert, *Sci. Rep.* **2024**, *14*, 14258.
[90] M. D. Murray, D. G. Nicholls, *Aust. J. Zool.* **1965**, *13*, 437.
[91] C. J. Steen, P. A. Carbonaro, R. A. Schwartz, *J. Am. Acad. Dermatol.* **2004**, *50*, 819.
[92] I. Herzog, P. Wohlsein, A. Preuss, S. N. Gorb, R. Pigeault, C. Ewers, E. Prenger-Berninghoff, U. Siebert, K. Lehnert, *Int. J. Parasitol. Parasites Wildl.* **2024**, *23*, 100898.
[93] W. Barthlott, M. Mail, C. Neinhuis, *Philos. Trans. R. Soc. London, Ser. A* **2016**, *374*, 20160191.
[94] G. McHale, M. I. Newton, N. J. Shirtcliffe, *Soft Matter* **2010**, *6*, 714.
[95] D. Neumann, D. Woermann, *Naturwissenschaften* **2009**, *96*, 933.
[96] J.-E. Melskotte, W. Barthlott, M. Brede, A. Leder, *Lasermethoden der Strömungsmesstechnik*, German Society For Laser Anemometry, Karlsruhe **2013**, pp. 1–7.
[97] P. Ditsche-Kuru, E. S. Schneider, J.-E. Melskotte, M. Brede, A. Leder, W. Barthlott, *Beilstein J. Nanotechnol.* **2011**, *2*, 137.
[98] Z. Cerman, B. F. Striffler, W. Barthlott, *Functional Surfaces in Biology*, Vol. *1*, (Ed: S. N. Gorb), Springer, Netherlands, **2009**, p. 97.
[99] W. H. Thorpe, D. J. Crisp, *J. Exp. Biol.* **1947**, *24*, 227.
[100] H. E. Hinton, *J. Insect Physiol.* **1976**, *22*, 1529.
[101] S. Vogel, *J. Biosci.* **2006**, *31*, 309.